

Highly accurate recalibrate waveforms for extreme-mass-ratio inspirals in effective-one-body frames

CHENG Ran^{1,2}, HAN Wen-biao^{1,2*}

(1. *Shanghai Astronomical Observatory, Chinese Academy of Sciences, Shanghai 200030, China;*

2. *University of Chinese Academy of Sciences, Beijing 100049, China)*

* *Corresponding author, E-mail: wbhan@shao. ac. cn*

Abstract: For the data analysis of space-based interferometers, calculating the gravitational waves of Extreme-mass-ratio-inspirals (EMRIs) in a highly accurate and efficient way is in high demand. In this paper, we present so-called “fully recalibrated waveform” for EMRIs with high accuracy. Based on the numerical data, by solving the Teukolsky equations, we recalibrate all of the mass-ratio independent coefficients of the factorized waveforms that are used in the effective-one-body (EOB) models. Due to these new coefficients with great efficiency (about 1 400 times more efficient than numerically solving the Teukolsky equations with the same computing environment), the precision of waveforms is improved enormously and is more accurate than other existing calibration models by at least one order in magnitude. For this reason, it meets the requirements of the space-based gravitational wave detection mission for the accuracy of EMRI waveform for uninclined, quasi-circular orbits. By investigating the dephasing value with our model, the spin of compact objects and the mass-ratio of the inspiralling system cannot be omitted in the waveform calculations. We believe our model will play an important role in the waveform-template construction of space-based GW detectors.

Key words: gravitational wave; EMRIs; waveform calculation

极端质量比旋进系统高精度重校准引力波建模

程 然^{1,2}, 韩文标^{1,2*}

(1. 中国科学院 上海天文台, 上海 200030; 2. 中国科学院大学, 北京 100049)

摘要: 针对空间引力波探测器的数据处理, 需高精度高效率计算极端质量比旋进系统引力波, 本文提出了一个完全重校准波形计算模型。该模型基于高精度 Teukolsky 方程数值求解的数据, 对等效单体问题的因子化波形中所有与质量比无关的系数进行重校准, 并利用重校准后的系数实现波形的高效计算 (相同计算环境下效率是 Teukolsky 方程数值求解的 1 400 倍)。其精度高于已有的校准模型精度至少一个量级, 可满足空间引力波探测器对于无轨道倾角准圆轨道 EMRI 波形的精度要求。文中还研究了致密天体的自旋以及旋进系统的质量比引起的相位偏移, 发现在波形计算中自旋和质量比均不可忽略。利用该模型对极端质量比旋进系统的波形实现高精度、高效率计算对于今后的空间引力波探测器波

收稿日期: 2018-06-04; 修订日期: 2018-07-07

基金项目: 国家自然科学基金 (No. 11773059) 资助

Supported by National Natural Science Foundation of China (No. 11773059)

形模版构建将发挥重大作用。

关键词: 引力波; 极端质量比旋进系统; 波形计算

中图分类号: O412.1; P145.8 **文献标识码:** A **doi:** 10.3788/CO.20191203.0441

1 Introduction

Extreme-mass-ratio-inspirals (EMRIs) are composed by supermassive black holes and stellar-mass compact bodies. For example, an EMRI event is that a compact body (stellarmassive black holes, neutron stars *etc.*) orbits around a supermassive black hole in a strong field zone the radius of an orbit shrinks due to the radiation of gravitational waves (GWs). People popularly believe that there are supermassive black-holes that reside in the centre of most galaxies^[1]. The typical mass of a supermassive blackhole ranges from about 10^5 to 10^7 solar masses (M_{\odot})^[2]. The frequency of GWs from EMRIs can be around $10^{-2} - 10^{-1}$ Hz when the small body's orbit is in the wildly relativistic region of the central black hole. EMRIs are very important gravitational wave sources for space-based detectors such as LISA^[3], Taiji^[4] and Tianqin^[5]. From the estimations of Refs. [6-9], LISA should see about 50 such EMRI events per year out to redshifts $z \approx 1$, based on calculations of stellar dynamics in galaxies' central cusps^[10].

Like LIGO, these space-based detectors also make use of matched-filtering technology to search the GW signals and analyze the properties and parameters of their sources. This requires a huge number of waveform templates in varied parameter space. Accurately and efficiently calculating the waveforms of EMRIs remains a challenge^[11]. Usually, one can calculate the waveforms accurately using numerical simulations (for example, numerically computing the blackhole perturbation equations^[12-14]), but computing speed is too slow to generate enough templates. Alternatively, one can use post-Newtonian approximation (including the hybrid method, see e. g. Refs. [15-17]) to quickly gener-

ate waveforms but doing so will invite a loss of accuracy in the strong field.

Considering the long time-scale of the waveforms of EMRIs, the requirement for accuracy and efficiency of waveforms is quite high. In the final year of the inspiral, an EMRI waveform has 10^5 circles^[9]. If we limit the dephase to be less than one circle between the theoretical templates and the real waveforms, the accuracy of the radiation reaction should be at 10^{-5} (the data analysis of the LISA mission demands that the phase of the extracted waveform be accurate to within a fraction of a radian over the entire inspiral^[11]). At the same time, the inspiral waveform depends on 14 different parameters^[18]. Based on the analysis of Ref. [9], if we assume that only about 8 of these 14 parameters affect phase evolution, it will need $10^{5 \times 8}$ templates to perform a fully coherent matched-filtering search for year-long inspiral waveforms.

In the LIGO's GW search, they used effective-one-body (EOB) models^[19-20] to construct waveform templates^[21]. These EOB waveforms are calibrated using numerical relativity data to guarantee accuracy. Because the EOB method is basically an analytical post-Newtonian (PN) formalism, the computing efficiency is very high. The EOBNR model works well in comparable mass-ratio binaries, but may not in the EMRIs. However, this inspires us to develop a similar waveform model in the EOB frame, *i. e.*, calibrating the waveform formalisms by the numerical Teukolsky-based data. The first attempt has been done by Yunes *et al.*^[22-23]. They calibrated several higher PN order coefficients to improve the accuracy of the factorized-resummed waveforms. However, up to now, most of the effort in calibrating the EOB and Phenom models has been concentrated on the (2,2) mode^[11]. As an attempt, we recalibrated all the coefficients in the factorized-resummed waveform for-

malisms and added a few higher order coefficients. In this sense, we call our method a fully recalibrated model. It will be seen that the accuracy of the waveforms improved greatly using our new recalibration.

This paper is organized as follows. In the next section, we introduce the original PN waveforms in the EOB frame. We then discuss our full recalibration method, our results and some comparisons in section III. At last, conclusions and remarks are given. Throughout the paper, we use units $G = c = 1$ and the metric signature $(-, +, +, +)$. Distance and time are measured by the central black-hole mass M .

2 Factorized-resummed EOB waveforms

To overcome the very poor convergence of the PN series (especially near the ISCO, *i. e.* innermost stable circular orbit) identified by Cutler *et al.* [24] and Poisson [25], Damour *et al.* suggested using resummation methods to extend the numerical validity of PN expansions (at least) up to the ISCO [26]. This technology was improved constantly (for example, see Refs. [27-29]) and formed the factorized-resummed PN waveforms, which aims at extending the validity of suitably resummed PN results beyond the ISCO and up to the merger. The waveforms were later introduced in the EOB approach and used to construct complete GW templates.

The factorized-resummed modes are

$$h_{lm} = h_{lm}^{\text{Newt}, \varepsilon_p} S_{lm}^{\varepsilon_p} T_{lm} e^{i\delta_{lm}} (\rho_{lm})^l, \quad (1)$$

where ε_p indicates the parity of the multipolar waveform, and $h_{lm}^{\text{Newt}, \varepsilon_p}$ is the Newtonian part. For the other terms as $S_{lm}^{\varepsilon_p}(v)$, $T_{lm}(v)$, $\delta_{lm}(v)$ and ρ_{lm} , we could refer to Refs. [27, 30] for detailed expressions. ρ_{lm} is a PN expansion about $(v/c)^n$. The numeric coefficients can be divided into four groups mass-ratio and spin independent; mass-ratio dependent; spin dependent; and mass-ratio and spin dependent coefficients. The energy fluxes down to in-

finitly \dot{E}^∞ can be expressed using the harmonically-decomposed waveforms h_{lm} from Ref. [31]:

$$\dot{E}^\infty = \sum_{l=2}^8 \sum_{m=1}^l \frac{\omega_m^2 |h_{lm}|^2}{8\pi}, \quad (2)$$

in this expression, $\omega_m = m\Omega$ where Ω is the orbital frequency. Now the PN waveforms are only expanded to multipoles $l=8$.

In the case of EMRIs, one can also add the energy fluxes down to their event horizons [22]. We calculate the flux through to the $N/2$ -th order Taylor expansion in PN theory [32]

$$\dot{E}^{\text{H}} = 32/5 v^2 v^{10} \sum_{n=0}^N [a_n(v) + b_n(v) \log(v)] v^n, \quad (3)$$

where ν is the symmetric mass-ratio which equals to $m_1 m_2 / (m_1 + m_2)^2$ (m_1 and m_2 are the masses of the two components), and v is the circular orbital frequency. Following reference [22], we classify the PN parameters based on their physical origins and conditions of spin inclusion. Those that correspond to radiation falling into the horizon will be labeled $(a_n^{\text{Hor}}, b_n^{\text{Hor}})$, with a superscript S(NS) if they are spin-dependent (spin-independent), where $a_{<14}^{\text{Hor}, \text{NS}}$, $b_n^{\text{Hor}, \text{NS}}$, $a_{<11}^{\text{Hor}, \text{S}}$ and $b_{<11}^{\text{Hor}, \text{S}}$ have been specified in reference [22]. For more details, see reference [33].

3 Fully recalibrated waveforms

Until now, the analytical forms of ρ_{lm} are expanded up to the 5PN order. For example

$$\rho_{22} = 1 + \left(\frac{55}{84}\nu - \frac{43}{42}\right)v^2 - \frac{2}{3}q\left(1 - \frac{\nu}{2}\right)v^3 + \dots, \quad (4)$$

where q is the dimensionless Kerr parameter $q \equiv J/M^2$, and J is the angular momentum of the black hole. As already shown in Ref. [22], the accuracy of these original waveforms is far from the requirement in the EMRI simulations (note that, even with the resummation method, it is not enough to solve the EOB problem because the improved Hamiltonian and radiation-reaction force are built from finite PN

expansions^[20]). Yunes *et al.* calibrated a few higher order coefficients to improve the accuracy of the resummed formalisms. In previous work^[34] by one of us, we fitted a set of polynomials from the Teukolsky-based fluxes to accurately calculate $\dot{E}^{\infty, \text{H}}$ and waveforms. In present work, we keep the forms of the factorized-resummed expansions, but recalibrate all numeric coefficients of these expansions. The reference data for recalibration are calculated using highly accurate solutions of the Teukolsky equations^[13-14]. The details of the Teukolsky equations and our numerical algorithm are addressed in our previous papers^[35-37] and the references inside.

For the recalibration, following Refs. [22-23, 27-28], we first write down the expressions of ρ_{lm} with undetermined numeric coefficients, for $m=l$,

$$\begin{aligned} \rho_{lm} = & 1 + a_1 v^2 + b_1 q v^3 + (a_2 + b_2 q^2) v^4 + b_3 q v^5 + \\ & [b_4 q^2 + a_3 + a_4 \text{eulerlog}(mv)] v^6 \\ & [b_5 q + b_6 q^3] v^7 + [b_7 q^2 + b_8 q^4 + a_5 + \\ & q_6 \text{eulerlog}(mv)] v^8 + (b_9 q + b_{10} q^3) v^9 + \\ & [a_7 + a_8 \text{eulerlog}(mv)] v^{10} + \\ & [a_9 + a_{10} \text{eulerlog}(mv)] v^{12}, \end{aligned} \quad (5)$$

where $\text{eulerlog}(mv) = \gamma_E + \log(2mv)$, $\gamma_E = 0.577215\cdots$ is Euler's constant, and for $m \neq l$,

$$\begin{aligned} \rho_{lm} = & 1 + b_1 q v + (a_1 + b_2 q^2) v^2 + (b_3 q + b_4 q^3) v^3 + \\ & (a_2 + b_5 q^2 + b_6 q^4) v^4 + \\ & (b_7 q + b_8 q^3 + b_9 q^5) v^5 + \\ & [a_3 + a_4 \text{eulerlog}(mv) + \\ & b_{10} q^2 + b_{11} q^4 + b_{12} q^6] v^6 + \\ & [b_{13} q + b_{14} \text{eulerlog}(mv) q + \\ & b_{15} q^3 + b_{16} q^5 + b_{17} q^7] v^7 + \\ & [a_5 + a_6 \text{eulerlog}(mv)] v^8 + \\ & [a_7 + a_8 \text{eulerlog}(mv)] v^{10} + \\ & [a_9 + a_{10} \text{eulerlog}(mv)] v^{12}, \end{aligned} \quad (6)$$

The coefficients a_1, a_2, a_3, \cdots are spin-independent, and those for b_1, b_2, b_3, \cdots are spin-dependent. Considering the small mass-ratio limit, all terms that depend on mass-ratio have been omitted.

To get all the numeric coefficients in Eqs. (5, 6), we adopt a two-dimensional (*i. e.*, in spin pa-

rameter q and orbital frequency v) least-squares method to suit them. The data for the least-squares fitting comes from the highly accurate Teukolsky-based fluxes. We have 17 groups of numerical data with varied spin parameters q : $-0.9, -0.7, -0.5, -0.3, -0.1, 0.0, 0.1, 0.2, 0.3, 0.4, 0.5, 0.6, 0.7, 0.75, 0.8, 0.85, 0.9$. Where a positive q means that the direction of spin of the Kerr black hole is in parallel with orbital angular momentum of the small object, and negative q means the anti-parallel case applies. Because the ISCO is closer to the black hole when q approaches 1, and because the variations of fluxes at this point are wilder, we insert two points $q = 0.75, 0.85$ between 0.7 and 0.9. For each q , we sample 18 points in the orbital frequency parameters, from $v \approx 0.02 \sim 0.08$ (depends on q) to the frequency at ISCO v_{ISCO} . These 18 points are generated by the Chebyshev nodes to obtain better performance on the boundary. Therefore, we have $17 \times 18 = 306$ sampling points in total on the two dimensional parameter space $\{q, v\}$. Combining Eq. (1) and Eq. (2), for each (l, m) mode, one has

$$\rho_{lm} = \left[\frac{\dot{E}_{lm}^{\infty}}{\omega_m^2 |h^{\text{Newt}, \varepsilon_p} S_{lm}^{\varepsilon_p} T_{lm}|} \right]^{1/l}. \quad (7)$$

The precise values of fluxes \dot{E}_{lm}^{∞} on these sampling points are provided by the numerical calculation of the Teukolsky equations. $\omega_n = m\Omega$, and Ω can be calculated from the relation $v = (M\Omega)^{1/3}$. All the other terms in the denominator can be directly calculated from the analytical expressions. If value of right hand side now is known, then one can solve for all coefficients in Eqs. (5, 6) by using the two-dimensional least-square method. All coefficients in ρ_m are listed in Tab. 1 – 3 of the Appendix.

To demonstrate the performances of these recalibration formalisms, we show the relative differences between our recalibrated fluxes and the Teukolsky-based ones in Fig. 1. From Fig. 1 we can see that the maximum relative error of our recalibrated fluxes is slightly larger than 1×10^{-4} . Compared to Fig. 1

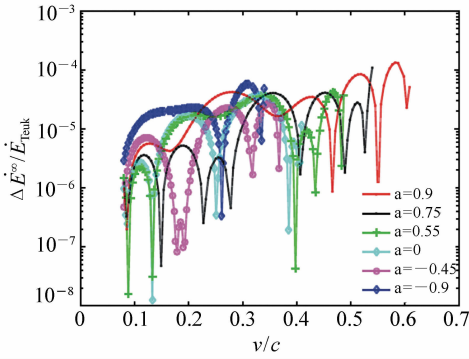


Fig. 1 Relative errors of the energy flux emissions to infinity, where $\Delta \dot{E}^\infty \equiv |\dot{E}_{\text{Teuk}}^\infty - \dot{E}_{\text{recal}}^\infty|$, $\dot{E}_{\text{recal}}^\infty$ are the recalibrated PN fluxes

in Ref. [23], we can see that our new formalisms are not only much better than the original factorized-resummation PN fluxes (relative errors are even larger than 10^{-1}), but also that they are a little better than the calibrated results of Yunes *et al.* [23] (maximum relative error approaches 10^{-3}). As expected, our model also has the advantage of being highly efficient by providing results of energy-flux for l from 2 to 8 in approximately 1.8 ms versus approximately 2.5 s when numerically solving the Teukolski equation for the same parameters.

However, based on the experiences in Ref. [23], only one order of improvement may be not enough for EMRI simulations with longer time scales. We find that it is very hard to achieve more accurate “global” coefficients that are valid for all q parameters. For better performance, the spin background is divided into 4 groups (see Tab. 1, and for each q group). Coefficients a_n and b_n in Eqs. (5) are fitted

by the least squares method for this group only. These grouped coefficients are listed in Tab. 4 of the Appendix. Note that we still use the “global” coefficients for the $m \neq l$ cases in Eq. (6). This is because $m = l$ modes are much more dominant than $m \neq l$ modes for the same l . The accuracy of fluxes is mainly determined by the $m = l$ modes. For simplicity, in the cases where $m \neq l$, we still use the “global” coefficients listed in Tab. 2 – 3 in the appendix for all q values. For some very unimportant modes (such as $l=4, m=l$), we directly use the original PN formalisms which can be found in Ref. [27].

The results of the recalibrated fluxes using the grouped coefficients in Tab. 4 from the appendix are shown in Fig. 2. We can now see that the relative precision is improved by one order of magnitude compared to that of the “global” coefficients. The maximum relative error is slightly larger than 1×10^{-5} . We can conclude that our recalibrated waveforms are more precise than the ones in Ref. [23] by about two orders of magnitude.

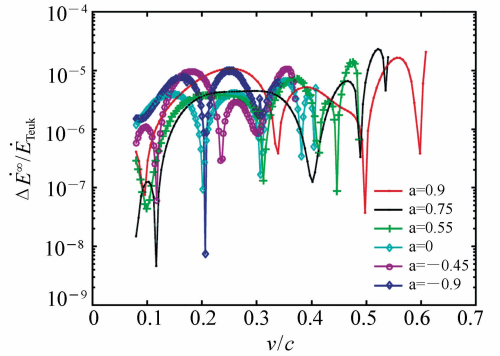


Fig. 2 Relative errors of the grouped-recalibration energy flux emissions to infinity

Tab. 1 Groups of $q(m=l)$

Group	I	II	III	IV
q	$-0.9 \sim -0.3$	$-0.3 \sim 0.3$	$0.3 \sim 0.7$	$0.7 \sim 0.9$

As we can see in Ref. [23], the PN formalisms for the energy fluxes absorbed by the event horizon are quite inaccurate. \dot{E}^{H} is also supposed to be cali-

brated as above according to Eq. (3) and the relevant explanation in our paper. To improve the performance in estimating the energy flux, $a_8^{\text{Hor,NS}}$,

$a_{10}^{\text{Hor,NS}}$ and $a_{12}^{\text{Hor,NS}}$ are firstly selected for refitting to correspondingly replace the original PN parameters for $q = 0$ with 18 data points by using the least-square method while keeping other parameters unchanged (for $a_{<8}^{\text{Hor,NS}} = a_9^{\text{Hor,NS}} = a_{11}^{\text{Hor,NS}} = a_{13}^{\text{Hor,NS}} = 0$). Then, under this precondition, we consider the parameter-fitting in $a_{11}^{\text{Hor,NS}}$ and $a_{12}^{\text{Hor,NS}}$ for $q = -0.9, -0.7, -0.5, -0.3, -0.1, 0, 0.1, 0.2, 0.3, 0.4, 0.5, 0.6, 0.7, 0.8$ and 0.9 , each having 18 data points. For simplicity, we adopt the following expressions for both terms and make p_n fitted:

$$\begin{aligned} a_{11}^{\text{Hor,S}} &= p_1 q + p_2 q^2 + p_3 q^3 + \\ & p_4 q^4 + p_5 q^5 + p_6 q^6 \\ a_{12}^{\text{Hor,S}} &= p_7 q + p_8 q^2 + p_9 q^3 + p_{10} q^4 + \\ & p_{11} q^5 + p_{12} q^6 + p_{13} q^7. \end{aligned} \quad (8)$$

The results are listed in Tab. 5 of the Appendix.

The comparison of the total PN fluxes with Teukolsky-based fluxes is shown in Fig. 3. We can see that the recalibrated formalisms for the energy fluxes down near the horizon are much more accurate than those with original coefficients. Compared with the Fig. 2 of Ref. [23], the accuracy of the total energy fluxes improved about two orders of magnitude.

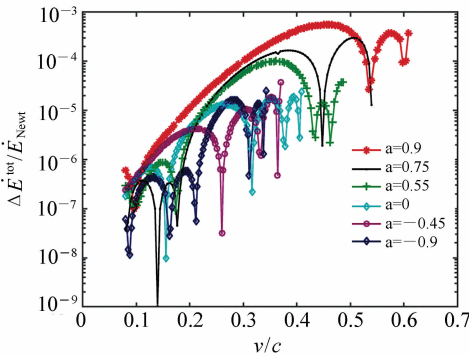


Fig. 3 Relative errors of the total energy fluxes which include the black hole absorption terms. $\dot{E}_{\text{Newt}} \equiv 32/5\nu^2 v^{10}$ is the leading-order (Newtonian) portion of the flux

Theoretically, the higher the precision of the fluxes, the more accurate the evolving waveforms.

To confirm the accuracy of the EOB model with our recalibrated waveforms, we choose a specific EMRI like the one in Ref. [23]. For simplicity, we just choose EMRIs with masses $M = 10^6 M_\odot$ and $m = 10 M_\odot$ for a mass ratio of 10^5 and inspirals of $\sim 10^5$ rads of orbital phase, depending on the spin. We take EMRI with spin background of $q = 0.9, 0$ and -0.9 and evolve them at an initial orbit radius of $r_0 = 11M$. The evolution lasts about 32 months for a small object that reaches the ISCO. Because the radius of an ISCO where $q = -0.9$ is about $9M$ (comparatively, the one with $q = 0.9$ is about $2.3M$), the EMRI evolves over about 8 months.

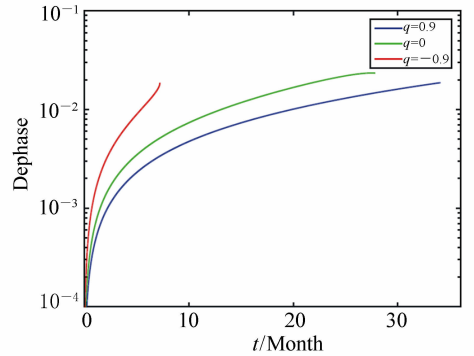


Fig. 4 Absolute value of the dephasing (in radians) computed in the recalibrated EOB model and the Teukolsky-based waveforms for the dominant $(l, m) = (2, 2)$ mode (in this system, $M = 10^6 M_\odot$ and $m = 10 M_\odot$). Different curves correspond to different background spin values. The cases where $q = 0$ and -0.9 stop earlier because they arrive at the ISCO earlier

The dephase of dominated $(2, 2)$ mode-waveforms calculated in the EOB frame with the newly recalibrated formalisms and the Teukolsky-based ones is shown in Fig. 4. During the whole evolution of all spin parameters, the dephase is less than 0.1 rad. This performance should satisfy the requirement for the data analysis of the EMRIs. The reason for our better performance for the dephase lies in the high accuracy of the total energy fluxes (including the black hole absorption term). We have two more orders of improvement on the accuracy of the fluxes

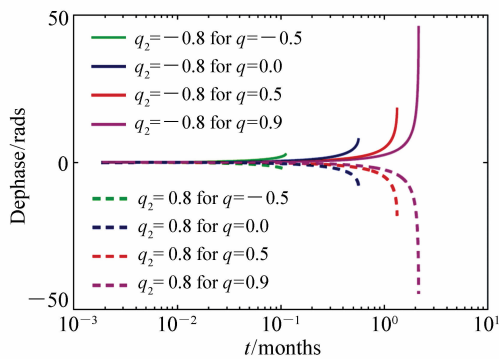


Fig. 5 Dephase (in radians) caused by the spin of the inspiraling particle computed in the recalibrated EOB model with the general case and the mass-ratio of 10^{-4} (where $M = 10^6 M_{\odot}$ and $m = 10^2 M_{\odot}$) for different spin parameters of the central black hole (in this case the mass-ratio does not vanish in the Hamiltonian terms and ρ_{lm})

compared with the results in Ref. [23]. This also induces two orders improvement in the dephase of the (2,2) mode, accordingly.

In Fig. 5 we illustrate the evolution of the dephasing value induced by the spin of the particle ($S_2 = mq_2$, where q_2 is the spin parameter of the particle) under various q conditions in the EOB frame. The evolution is initiated at a position where the frequency of the waveform observed is about 2.6 MHz and is terminated at about the ISCO. The value of q_2 is chosen to be 0.8 and -0.8 in order to examine the rough magnitude of this effect on dephase and the corresponding effect from S_2 -direction. It is clear that the maximum dephasing value approaches 50 rads when q is 0.9. The opposite S_2 -direction plays an adverse role on the dephasing value.

The magnitude of the dephase due to the mass-ratio is also shown in Fig. 6. The example we adopt here is the “test particle model” (TP model) that is referred to as an approximation scheme in which the mass-ratio vanishes in ρ_{lm} and the Hamiltonian terms except with dp_{φ}/dt . Moreover, as the energy flux is determined by the mass-ratio, the evolution appears longer with an increase of ν . However, the total

dephasing value seems unchanged at the ISCO.

As can be seen from the evolution of the dephasing value, the magnitude induced by each factor is accurately described by our recalibrated EOB model (when using the Teukolsky-based one as a standard). The spin of a compact object and the mass-ratio of the inspiraling system is of high impact (for instance, if the precondition: dephasing value $< \pi$ is needed, then the time of evolution should not exceed one month where $\nu = 10^{-5}$ for some value of q with the adopted approximation scheme) and its influence should not be neglected in data analysis.

4 Conclusions

The successes of the EOB model in the precise simulation of waveforms from comparable mass-ratio binaries motivated us to develop waveform models for extreme-mass-ratio inspirals in the EOB framework. At present, to improve the accuracy of factorized-resummation PN waveforms, we recalibrated all the spin-independent and -dependent coefficients of the PN waveform formalisms.

Firstly, we calibrated the global coefficients, which are valid for all q spin parameters by using 17 groups of numerical Teukolsky-based flux data with $q = -0.9, -0.7, -0.5, -0.3, -0.1, 0.0, 0.1, 0.2, 0.3, 0.4, 0.5, 0.6, 0.7, 0.75, 0.8, 0.85, 0.9$. This improves the accuracy of fluxes by about one order of magnitude compared with the previous results, as in Ref. [23]. For better waveform formalisms, we divided the spin background into four groups. For each group, we calibrated the coefficients. In this way, we improved the accuracy of the fluxes to about two orders higher than the previous results. Further more, we also calibrated a few of the coefficients for the PN expressions of the energy-fluxes down to the horizon. This improves the accuracy of total energy fluxes greatly. All these coefficients for calculation and validation are listed in

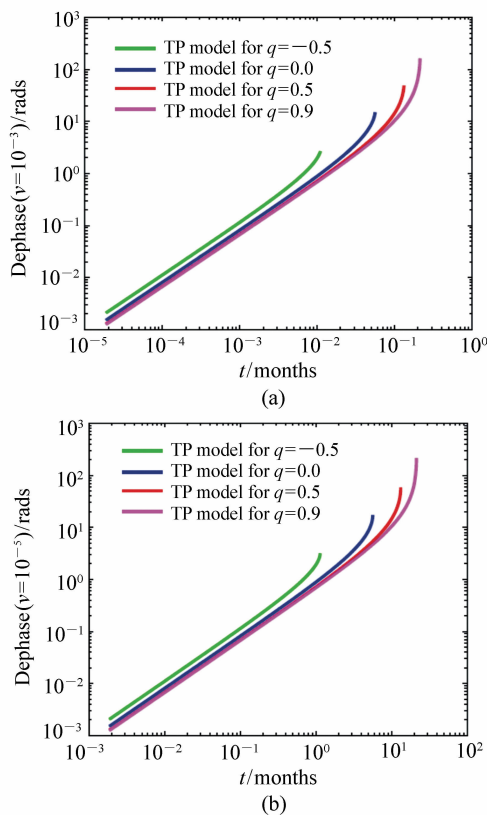


Fig. 6 The dephase (in radians) induced by the “test-particle model” (compared with the general-case) with a mass-ratio of 10^{-3} (subgraph (a), where $M = 10^6 M_{\odot}$ and $m = 10^3 M_{\odot}$) and 10^{-5} (subgraph (b), where $M = 10^6 M_{\odot}$ and $m = 10 M_{\odot}$)

Tab. 1–4 from the Appendix. To assess the quality of the waveform model in the EMRI system, the Teukolsky-based waveform was reasonably treated as “exact”, as demonstrated in Ref. [16]. As for the validity of our code which generates the relevant Teukolsky-based numerical data for parameter-recalibration and flux-comparison, please refer to Ref. [35] for more details. In light of the discussion above, the accuracy of our waveform illustrated in Fig. 1–3 is definitely reliable.

With the recalibrated PN formalisms, we could accurately evolve the orbits of EMRIs in the EOB frame, and simultaneously obtain the waveforms. In this way, the computation efficiency was much high-

er (about 1 400 times faster in our case) than solving the Teukolsky equation numerically. For example, we calculated the dephasing of the (2,2) mode between the recalibrated waveforms and the Teukolsky-based ones for an EMRI. As we could see, the dephasing was less than 0.1 rads, even for evolutionary waveforms that spanned more than 30 months. We think that the performance of the recalibrated waveforms in the EOB frame meet the requirement of the waveform templates of the EMRIs for space-based GW detectors. With these new waveforms, we could calculate the waveforms of EMRIs for long time-scales with accuracy and efficiency. We believe that our recalibrated formalisms can replace the Teukolsky-based waveforms in future data analysis.

As an application of our model, we investigated the spin of compact objects and the mass-ratio of the inspiraling system under a mass-ratio-related approximation scheme and their effect on the dephasing value during evolution using our model. The results showed that they are considerable in both magnitude and in time span, which should catch our attention in the data analysis.

However, there are at least three points that may help further improve the results in the present research. First, one can add more (l, m) modes. In this paper, we only consider the modes up to $l = 8$. For higher modes, one can write down the similar formalisms, then calibrate the coefficients from numerical data. Second, one may find a better way to calibrate the fluxes down to the horizon of black hole. Third, the recalibration model is currently confined to the case of circular, equatorial orbits, thus could be extended to more generic orbits.

Efficiency and accuracy are both highly valued in the search for the GWs of EMRIs. We believe our recalibration model will contribute to the waveform-template construction of space-based GW detectors, and play a role in promoting the development of gravitational wave astronomy.

Appendix

Tab. 1 The coefficients of $m = l$ modes which are valid for arbitrary spin parameters

(l, m)	(2, 2)	(3, 3)	(4, 4)	(5, 5)	(6, 6)	(7, 7)	(8, 8)
a1	-1.022 468 181 7E+00	-1.166 063 960 2E+00	-1.222 356 37E+00	-1.248 446 73E+00	-1.261 692 97E+00	-1.268 734 25E+00	-1.272 515 18E+00
a2	-2.556 630 282 3E+00	-1.982 233 742 5E+00	-1.797 768 05E+00	-1.716 611 88E+00	-1.671 145 78E+00	-1.642 913 77E+00	-1.623 687 30E+00
a3	-2.989 362 917 8E+01	1.777 643 876 1E+01	2.886 247 18E+01	3.337 564 34E+01	3.577 383 61E+01	3.734 903 96E+01	3.847 593 79E+01
a4	-1.321 863 979 3E+02	-6.496 732 141 8E+01	-4.359 364 35E+01	-3.458 434 47E+01	-2.943 673 66E+01	-2.617 925 16E+01	-2.390 323 07E+01
a5	3.003 861 000 9E+03	2.217 282 903 4E+03	1.806 549 41E+03	1.622 294 08E+03	1.507 914 88E+03	1.434 376 85E+03	1.382 208 86E+03
a6	-3.890 299 901 0E+03	-1.898 295 906 6E+03	-1.242 600 28E+03	-9.693 349 89E+02	-8.139 852 99E+02	-7.159 489 95E+02	-6.477 228 59E+02
a7	2.834 727 515 5E+04	1.726 656 885 0E+04	1.282 883 64E+04	1.095 918 71E+04	9.86577323E+03	9.17631339E+03	8.69764708E+03
a8	-1.639 831 498 1E+04	-8.112 548 558 9E+03	-5.307 193 33E+03	-4.150 991 20E+03	-3.495 828 34E+03	-3.083 424 48E+03	-2.797 365 44E+03
a9	2.440335915E+04	1.381 920 273 7E+04	9.782 378 74E+03	8.115 062 78E+03	7.154 460 08E+03	6.549 786 13E+03	6.130 943 60E+03
a10	-7.977 993 020 0E+03	-3.997 260 949 3E+03	-2.611 899 06E+03	-2.045 055 93E+03	-1.723 844 44E+03	-1.521 664 07E+03	-1.381 520 64E+03
b1	-6.654 444 310 9E-01	-6.657 707 852 3E-01	-6.655 054 65E-01	-6.653 500 32E-01	-6.652 170 80E-01	-6.651 032 66E-01	-6.650 044 89E-01
b2	4.839 556 166 3E-01	4.921 897 888 1E-01	4.957 273 96E-01	4.977 599 98E-01	4.990 639 17E-01	5.000 077 43E-01	5.007 466 43E-01
b3	-1.596 446 922 1E+00	-1.309 300 627 5E+00	-1.250 037 24E+00	-1.246 528 03E+00	-1.260 877 52E+00	-1.28 0495 56E+00	-1.300 879 58E+00
b4	5.734 839 505 4E-01	2.283 136 207 1E-01	9.327 794 42E-02	2.127 795 16E-02	-2.084 178 97E-02	-4.860 719 28E-02	-6.857 293 72E-02
b5	1.789 698 922 8E+00	2.019 415 567 5E+00	2.271 882 77E+00	2.432 800 65E+00	2.545 662 28E+00	2.631 230 38E+00	2.699 362 03E+00
b6	-4.327512994E-01	-4.697 274 956 1E-03	1.037 468 12E-01	1.497 761 45E-01	1.727 957 43E-01	1.855 015 88E-01	1.930 142 84E-01
b7	1.439 338 856 4E+00	-2.034 145 921 6E-01	-3.306 731 29E-01	-2.517 563 90E-01	-1.468 729 26E-01	-3.891 878 43E-02	6.461 840 54E-02
b8	-8.219 009 282 8E-01	-3.369 305 813 1E-01	-2.533 886 63E-01	-2.129 2821 5E-01	-1.895 455 37E-01	-1.749 856 42E-01	-1.651 220 42E-01
b9	-1.945 096 581 0E+01	-1.153 450 623 2E+01	-1.048 765 34E+01	-1.043 332 29E+01	-1.063 653 20E+01	-1.092 611 79E+01	-1.123 849 02E+01
b10	7.257 863 585 9E+00	3.789 085 707 6E+00	2.943 875 32E+00	2.554 989 47E+00	2.344 425 89E+00	2.216 450 86E+00	2.131 647 91E+00

Tab. 2 The coefficients of $m \neq l$ modes which are valid for arbitrary spin parameters

(l, m)	(2, 1)	(3, 2)	(3, 1)	(4, 3)	(4, 2)	(5, 4)	(5, 3)
a1	-1.052 770 768 5E+00	-1.214 524 079 1E+00	-7.215 243 63E-01	-1.261 237 224 7E+00	-8.679 860 98E-01	-1.278 159 339 1E+00	-9.613 795 17E-01
a2	-9.324 146 275 6E-01	-8.592 359 993 3E-01	-3.111 138 95E-01	-8.993 319 722 3E-01	-4.681 233 60E-01	-9.703 447 884 9E-01	-6.731 221 87E-01
a3	-1.675 907 847 6E+01	3.195 184 522 1E+00	-7.487 837 60E+01	4.570 736 449 4E+00	-5.328 428 12E+00	2.8215508168E+00	6.604 643 86E+00
a4	-1.866 925 338 7E+01	2.1653247307E+00	-7.293 641 37E+01	1.2609902334E+01	-2.567 454 00E+01	1.261 197 025 9E+01	-2.305 766 46E+01
a5	-5.649 576 992 6E+01	-1.8136285648E+01	1.071 232 33E+02	-3.953 327 055 2E+02	5.930 784 62E+02	-5.259 624 937 6E+02	8.053 501 80E+02
a6	-7.026 626 158 4E+02	-1.608 723 142 1E+02	-2.356 214 09E+03	2.422 543 022 1E+02	-8.125 414 32E+02	3.0038340199E+02	-7.089 929 89E+02
a7	3.582 975 744 6E+03	2.607 784 185 2E+03	1.065 290 90E+04	-7.2699350331E+02	6.307 948 99E+03	-1.766 190 415 9E+03	6.821 782 59E+03
a8	-4.072 367 964 9E+03	-1.8307910870E+03	-1.061 043 76E+04	1.5064300121E+02	-3.740 910 23E+03	6.077 441 133 5E+02	-3.260 189 05E+03
a9	5.895 914 952 2E+03	4.0759893996E+03	1.278 645 27E+04	8.613 538 008 4E+02	5.93846520E+03	-2.428 063 956 7E+02	5.865 753 94E+03
a10	-2.6369522589E+03	-1.416 189 295 2E+03	-5.466 732 44E+03	-2.997 659 405 1E+02	-1.964 094 28E+03	3.2316814336E+01	-1.710 891 35E+03
b1	-7.498 459 329 6E-01	-4.444 274 746 5E-01	1.489 391 69E-05	-3.125 286 683 4E-01	2.647 462 47E-05	-2.400 546 485 3E-01	8.637 496 12E-06
b2	-2.839 848 709 1E-01	-1.993 845 606 9E-01	-1.487 913 60E-04	-1.477 055 182 2E-01	6.534 131 16E-06	-1.160 784 388 9E-01	1.229 922 70E-04
b3	1.747 103 0 80 5E+00	9.5894558412E-01	-1.855 297 18E+00	5.615 761 219 8E-01	-1.421 087 48E+00	3.220 733 346 7E-01	-1.181 170 99E+00
b4	-2.058 311 481 1E-01	-1.452 405 739 7E-01	7.593 551 10E-03	-1.061 982 134 6E-01	6.023 156 54E-03	-8.253 777 360 0E-02	5.701 244 10E-03
b5	-3.848 381 458 4E-01	1.053 911 289 0E-01	9.258 085 33E-01	2.572 512 640 7E-01	6.916 928 47E-01	3.301 909 793 5E-01	5.825 528 38E-01
b6	-1.735 803 594 3E-01	-1.234 845 195 2E-01	2.401 484 37E-02	-9.053 306 463 3E-02	1.996 986 76E-02	-7.114 902 281 7E-02	1.697 433 69E-02
b7	-1.025 372 823 5E+00	-1.451 572 848 2E+00	-1.183 304 13E+00	-1.602 668 884 0E+00	-7.516 288 71E-01	-1.695 667 401 9E+00	-7.465 129 58E-01
b8	2.118 001 110 0E-01	7.982 770 522 2E-02	-4.839 428 69E-02	2.541 511 106 5E-02	-3.612 392 91E-02	3.905 512 823 6E-03	-5.038 559 88E-02
b9	-3.277 598 703 9E-01	-1.962 138 611 3E-01	-1.332 059 30E-01	-1.323 999 540 7E-01	-1.131 302 56E-01	-9.795 818 720 1E-02	-9.312 859 92E-02
b10	3.840 876 660 1E+00	1.9580717285E+00	6.859 871 90E-01	1.275 477 884 9E+00	4.377 747 19E-01	9.275 896 964 0E-01	3.706 435 02E-01
b11	1.898 117 342 3E-01	9.9713522137E-02	5.662 333 93E-02	5.734 332 634 4E-02	1.393 423 13E-02	4.128 251 937 6E-02	3.809 151 54E-03
b12	-3.760 058 326 8E-01	-2.135 188 340 9E-01	-2.359 482 86E-01	-1.370 375 958 1E-01	-1.830 564 10E-01	-9.525 244 348 9E-02	-1.511 390 10E-01
b13	-5.408 315 532 8E+00	-3.464 904 458 5E-01	-5.408 792 77E-01	4.2430865177E+00	1.408 585 63E+00	8.035 869 836 0E+00	4.002 746 44E+00
b14	3.880 502 809 3E+00	-8.616 603 319 7E-01	-3.403 280 42E+00	-2.948 588 805 2E+00	-2.758 882 78E+00	-4.219 616 783 6E+00	-3.382 162 03E+00
b15	-1.842 975 192 3E+00	-4.374 448 220 6E-01	1.442 549 57E+00	5.469 939 110 7E-02	9.175 048 99E-01	2.777 109 115 4E-01	8.199 623 57E-01
b16	1.830 246 385 7E+00	9.950 914 027 5E-01	5.428 113 90E-01	6.292 281 918 2E-01	6.257 180 75E-01	4.408 837 023 4E-01	5.069 086 53E-01
b17	-7.231 239 134 3E-01	-4.477 417 454 9E-01	3.762 655 31E-01	-3.026 738 627 0E-01	2.073 868 92E-01	-2.200 669 712 7E-01	1.767 621 32E-01

Tab. 3 The coefficients of $m \neq l$ modes which are valid for arbitrary spin parameters(continued from the previous Table)

(l, m)	(6,5)	(6,4)	(7,6)	(7,5)	(8,7)	(8,6)
a1	-1.284 669 626 4E+00	-1.023 686 54E+00	-1.286 885 692 6E+00	-1.067 186 06E+00	-1.287 156 405 3E+00	-1.098 629 59E+00
a2	-1.028 085 358 6E+00	-8.018 141 73E-01	-1.074 299 838 6E+00	-8.729 259 81E-01	-1.112 844 024 7E+00	-9.493 332 28E-01
a3	1.472 347 159 8E+00	1.331 757 94E+01	3.538 912 110 1E-01	1.470 839 95E+01	-4.483 256 765 8E-01	1.681 129 21E+01
a4	1.233 619 655 0E+01	-1.949 464 27E+01	1.211 704 144 4E+01	-1.334 258 45E+01	1.177 919 725 6E+01	-1.095 846 19E+01
a5	-6.295 934 462 4E+02	8.256 516 91E+02	-7.202 933 852 4E+02	6.449 319 28E+02	-7.913 400 649 7E+02	5.133 524 47E+02
a6	3.317 760 482 5E+02	-5.805 996 54E+02	3.543 042 634 6E+02	-4.002 443 63E+02	3.670 096 018 6E+02	-2.817 181 47E+02
a7	-2.554 337 752 5E+03	6.363 796 05E+03	-3.221 407 957 7E+03	5.017 946 87E+03	-3.743 105 003 4E+03	3.635 410 10E+03
a8	8.825 612 315 5E+02	-2.672 757 82E+03	1.080 513 340 4E+03	-1.940 072 55E+03	1.213 302 355 1E+03	-1.302 454 87E+03
a9	-1.035 957 835 9E+03	5.200 570 93E+03	-1.672 525 626 2E+03	4.094 932 64E+03	-2.163 146 999 8E+03	2.769 624 85E+03
a10	2.394 108 437 0E+02	-1.398 835 46E+03	3.884 784 872 8E+02	-1.041 371 23E+03	4.930 809 690 9E+02	-6.697 859 19E+02
b1	-1.945 164 876 5E-01	-9.276 115 11E-06	-1.633 498 982 9E-01	-2.038 498 55E-05	-1.407 190 719 5E-01	-3.844 786 49E-05
b2	-9.515 748 050 1E-02	2.027 543 61E-04	-8.042 045 305 6E-02	2.429 559 19E-04	-6.952 745 576 7E-02	2.947 547 50E-04
b3	1.616 957 762 2E-01	-1.037 429 03E+00	4.672 632 203 4E-02	-9.452 610 92E-01	-3.973 763 880 8E-02	-8.822 969 64E-01
b4	-6.696 064 958 1E-02	5.275 095 39E-03	-5.603 822 042 2E-02	4.441 613 54E-03	-4.798 581 364 9E-02	4.472 312 63E-03
b5	3.713 537 497 2E-01	5.269 446 85E-01	3.970 585 853 1E-01	4.974 969 77E-01	4.142 646 130 1E-01	4.795 464 35E-01
b6	-5.880 191 795 7E-02	1.384 682 88E-02	-5.035 312 483 9E-02	9.851 393 53E-03	-4.423 774 113 6E-02	8.134 474 34E-03
b7	-1.761 680 654 6E+00	-8.303 057 98E-01	-1.811 577 697 2E+00	-9.222 636 92E-01	-1.851 033 718 8E+00	-1.025 660 83E+00
b8	-8.913 465 222 1E-03	-5.772 940 54E-02	-1.798 016 664 8E-02	-5.328 945 31E-02	-2.514 783 323 2E-02	-6.246 975 95E-02
b9	-7.656 351 667 3E-02	-7.714 853 62E-02	-6.221 179 635 7E-02	-6.604 892 80E-02	-5.198 227 811 6E-02	-5.512 043 24E-02
b10	7.262 728 764 7E-01	3.360 048 80E-01	5.989 234 342 0E-01	3.021 497 74E-01	5.131 412 395 0E-01	2.827 435 30E-01
b11	3.334 719 854 0E-02	-1.008 563 04E-03	2.858 141 839 6E-02	7.366 687 00E-03	2.518 675 868 1E-02	-1.145 914 59E-03
b12	-6.882 351 666 3E-02	-1.236 445 70E-01	-5.083 061 206 8E-02	-1.021 380 72E-01	-3.788 455 622 6E-02	-8.186 363 93E-02
b13	1.123 533 316 8E+01	6.663 174 11E+00	1.396 627 392 5E+01	8.965 918 11E+00	1.633 311 534 2E+01	1.148 134 38E+01
b14	-5.115 762 205 6E+00	-4.044 250 61E+00	-5.785 792 946 0E+00	-4.541 680 77E+00	-6.308 317 376 1E+00	-5.126 363 20E+00
b15	4.119 160 672 2E-01	7.794 020 04E-01	5.035 774 531 5E-01	7.302 170 85E-01	5.716 361 550 8E-01	7.585 683 87E-01
b16	3.254 993 908 4E-01	4.118 102 02E-01	2.488 170 838 3E-01	3.422 348 73E-01	1.946 094 600 7E-01	2.750 452 22E-01
b17	-1.683 854 673 1E-01	1.501 910 73E-01	-1.338 063 291 4E-01	1.280 367 06E-01	-1.093 677 281 1E-01	1.113 988 36E-01

Tab. 4 The coefficients of $m = l$ modes based on grouped scheme of q

$q \in [-0.9, -0.3]$							
(l, m)	(2,2)	(3,3)	(4,4)	(5,5)	(6,6)	(7,7)	(8,8)
a1	-1.0238324589E+00	-1.1666709303E+00	-1.22272692E+00	-1.24871128E+00	-1.26189710E+00	-1.26889946E+00	-1.27265256E+00
a2	-1.9322199595E+00	-1.6982239660E+00	-1.60902141E+00	-1.57637497E+00	-1.55572345E+00	-1.54327211E+00	-1.53515569E+00
a3	1.6776389322E+01	1.3522892311E+01	1.52343985E+01	1.59397414E+01	1.68469663E+01	1.76268760E+01	1.83115555E+01
a4	1.5479500994E+00	-4.5947443723E+00	-1.53361972E+00	-4.60682085E+00	-4.63210420E+00	-4.65496324E+00	-4.67896082E+00
a5	-1.8192624506E+02	4.4491319332E+01	-1.63486330E+02	9.61889434E+01	1.12861272E+02	1.27440952E+02	1.41141272E+02
a6	3.2194663895E+02	-1.1723638062E+02	1.49851451E+02	-8.81108308E+01	-8.67098630E+01	-8.68703322E+01	-8.79866887E+01
a7	-2.8278341579E+03	3.1460308602E+03	-2.74939294E+03	2.37755084E+03	2.41794886E+03	2.52894255E+03	2.68274200E+03
a8	1.1598395745E+03	-2.2182522609E+03	1.33145017E+03	-1.13484716E+03	-1.04550190E+03	-1.01878762E+03	-1.02397840E+03
a9	3.8601428713E+03	1.1817432401E+04	-4.40918219E+03	5.59282833E+03	5.10341458E+03	5.03984615E+03	5.20453936E+03
a10	-2.1967780648E+03	-4.1773977137E+03	1.29946841E+03	-1.61518616E+03	-1.38602416E+03	-1.30771783E+03	-1.30378969E+03
b1	-6.6793229453E-01	-6.6720424772E-01	-6.66774242E-01	-6.66644827E-01	-6.66590257E-01	-6.66567923E-01	-6.66561334E-01
b2	4.8236679011E-01	4.9366060333E-01	4.98425955E-01	4.99738762E-01	5.00319603E-01	5.00535784E-01	5.00576061E-01
b3	-1.6020559274E+00	-1.2881524285E+00	-1.21738255E+00	-1.20711300E+00	-1.21573028E+00	-1.23054412E+00	-1.24680364E+00
b4	6.1743192155E-01	2.3025279218E-01	5.16814594E-02	1.62684669E-03	-2.54980053E-02	-3.73635438E-02	-4.17164909E-02
b5	1.8780950213E+00	1.7736706475E+00	1.94668881E+00	2.08945280E+00	2.14658974E+00	2.18035290E+00	2.20130345E+00
b6	-1.7550106249E+00	-3.5013764659E-01	2.22683987E-01	4.85011544E-01	5.69072581E-01	6.02287370E-01	6.10935151E-01
b7	-1.0884445891E+01	-4.4636616536E+00	-7.66607740E-01	6.37091381E-01	1.17940168E+00	1.41214060E+00	1.49317225E+00
b8	-5.7896351908E+00	-2.0368987537E+00	-3.66538715E-01	3.23664389E-01	5.61783870E-01	6.56074183E-01	6.80942539E-01
b9	-3.0477571172E+01	-1.4349875807E+01	-9.91550018E+00	-8.69174348E+00	-8.27754688E+00	-8.22015261E+00	-8.32555589E+00
b10	-2.0952037398E+01	-6.6926746183E+00	3.41832098E-01	2.99617757E+00	3.96572457E+00	4.34529193E+00	4.44120523E+00

(continue)

$q \in [-0.3, 0.3]$							
(l, m)	(2,2)	(3,3)	(4,4)	(5,5)	(6,6)	(7,7)	(8,8)
a1	-1.023 911 645 4E+00	-1.166 704 782 4E+00	-1.222 750 37E+00	-1.248 736 07E+00	-1.261 921 19E+00	-1.268 923 63E+00	-1.272 677 14E+00
a2	-1.863 038 361 5E+00	-1.668 391 076 2E+00	-1.596 688 90E+00	-1.562 546 46E+00	-1.543 337 72E+00	-1.531 274 47E+00	-1.523 041 24E+00
a3	3.322 718 074 0E+01	1.665 960 902 2E+01	1.469 504 60E+01	1.455 681 49E+01	1.469 438 44E+01	1.479 829 30E+01	1.480 878 08E+01
a4	2.730 630 887 8E+01	7.224 840 921 1E+00	2.583 051 56E+00	9.239 429 39E-01	3.198 615 48E-01	1.394 039 00E-01	1.604 289 30E-01
a5	-8.304 618 864 7E+02	-5.422 406 825 0E+02	-4.061 496 10E+02	-3.470 934 58E+02	-3.352 356 81E+02	-3.483 629 05E+02	-3.763 340 64E+02
a6	1.794 927 232 3E+03	6.091 326 360 5E+02	3.390 354 31E+02	2.397 797 17E+02	2.034 933 68E+02	1.925 152 03E+02	1.935 576 10E+02
a7	-1.986 790 362 0E+04	-8.396 711 985 1E+03	-5.251 431 11E+03	-3.930 210 15E+03	-3.483 039 94E+03	-3.439 753 85E+03	-3.614 761 37E+03
a8	1.389 486 446 5E+04	4.513 748 998 7E+03	2.421 231 26E+03	1.620 222 29E+03	1.323 075 84E+03	1.229 12 771E+03	1.232 020 48E+03
a9	-3.360 589 053 6E+04	-1.193 004 353 7E+04	-6.689 183 91E+03	-4.425 562 66E+03	-3.577 644 35E+03	-3.352 227 86E+03	-3.449 934 03E+03
a10	1.213 431 060 6E+04	3.720 835 603 4E+03	1.900 692 86E+03	1.166 709 00E+03	8.903 283 31E+02	7.990 393 70E+02	7.962 688 14E+02
b1	-6.625 553 460 8E-01	-6.651 912 993 1E-01	-6.658 312 68E-01	-6.660 258 53E-01	-6.660 908 22E-01	-6.661 035 06E-01	-6.660 917 86E-01
b2	5.084 738 194 4E-01	5.018 306 197 2E-01	4.989 082 98E-01	4.979 033 35E-01	4.974 503 02E-01	4.972 307 13E-01	4.971 292 27E-01
b3	-1.759 096 174 7E+00	-1.349 399 188 2E+00	-1.249 253 83E+00	-1.229 357 96E+00	-1.234 707 25E+00	-1.248 672 15E+00	-1.265 221 69E+00
b4	-4.228 398 000 8E-02	5.589 578 425 3E-03	1.932 915 87E-02	1.654 706 96E-02	1.383 552 33E-02	1.188 070 41E-02	1.036 135 92E-02
b5	3.800 658 995 0E+00	2.511 213 247 5E+00	2.284 034 34E+00	2.248 297 72E+00	2.253 596 05E+00	2.271 285 04E+00	2.293 095 04E+00
b6	7.291 799 468 6E-02	2.475 215 605 0E-01	2.851 465 96E-01	2.968 030 52E-01	3.023 491 95E-01	3.051 348 15E-01	3.065 048 92E-01
b7	4.502 358 337 8E+00	8.622 007 126 1E-01	1.762 336 68E-03	-2.577 196 07E-01	-3.428 246 24E-01	-3.586 613 01E-01	-3.431 554 94E-01
b8	-1.023 911 645 4E+00	-1.166 704 782 4E+00	-1.222 750 37E+00	-1.248 736 07E+00	-1.261 921 19E+00	-1.268 923 63E+00	-1.272 677 14E+00
b9	-1.863 038 361 5E+00	-1.668 391 076 2E+00	-1.596 688 90E+00	-1.562 546 46E+00	-1.543 337 72E+00	-1.531 274 47E+00	-1.523 041 24E+00
b10	3.322 718 074 0E+01	1.665 960 902 2E+01	1.469 504 60E+01	1.455 681 49E+01	1.469 438 44E+01	1.479 829 30E+01	1.480 878 08E+01
$q \in [0.3, 0.7]$							
(l, m)	(2,2)	(3,3)	(4,4)	(5,5)	(6,6)	(7,7)	(8,8)
a1	-1.023 975 806 0E+00	-1.166 721 080 0E+00	-1.222 793 16E+00	-1.248 781 15E+00	-1.261 966 02E+00	-1.268 970 16E+00	-1.272 725 61E+00
a2	-1.773 785 209 4E+00	-1.632 220 902 1E+00	-1.548 886 17E+00	-1.513 749 41E+00	-1.492 723 26E+00	-1.478 671 22E+00	-1.468 500 69E+00
a3	3.318 171 742 4E+01	1.485 007 940 2E+01	1.120 821 58E+01	8.742 441 37E+00	6.565 451 17E+00	4.463 981 92E+00	2.400 700 48E+00
a4	3.953 835 298 8E+01	1.245 654 120 0E+01	1.270 989 48E+01	1.188 358 51E+01	1.193 903 80E+01	1.230 958 59E+01	1.279 855 97E+01
a5	-1.104 050 524 8E+03	-6.678 847 665 8E+02	-8.642 866 09E+02	-9.540 746 77E+02	-1.067 275 14E+03	-1.188 128 91E+03	-1.310 196 08E+03
a6	1.765 670 955 2E+03	6.364 340 267 5E+02	6.480 557 78E+02	6.118 247 35E+02	6.123 512 91E+02	6.261 317 50E+02	6.450 250 23E+02
a7	-1.584 521 768 6E+04	-7.018 461 656 8E+03	-8.233 063 96E+03	-8.510 535 42E+03	-9.126 263 28E+03	-9.861 459 69E+03	-1.063 491 43E+04
a8	1.007 746 475 7E+04	3.520 695 972 9E+03	3.616 055 48E+03	3.402 394 51E+03	3.400 016 59E+03	3.474 231 99E+03	3.578 477 07E+03
a9	-1.943 757 060 3E+04	-7.516 377 183 0E+03	-8.463 821 74E+03	-8.439 697 62E+03	-8.831 046 55E+03	-9.372 034 96E+03	-9.967 170 90E+03
a10	6.701 134 943 0E+03	2.262 034 338 1E+03	2.348 297 02E+03	2.20 493 971E+03	2.202 448 11E+03	2.251 088 77E+03	2.319 908 21E+03
b1	-6.733 755 278 4E-01	-6.696 972 546 1E-01	-6.691 529 88E-01	-6.690 190 65E-01	-6.690 404 96E-01	-6.691 115 33E-01	-6.691 907 72E-01
b2	5.843 602 324 0E-01	5.360 214 944 8E-01	5.281 348 98E-01	5.259 445 81E-01	5.257 183 07E-01	5.262 380 99E-01	5.270 649 02E-01
b3	-1.662 151 538 5E+00	-1.308 471 947 2E+00	-1.225 235 87E+00	-1.209 000 88E+00	-1.214 680 96E+00	-1.227 731 14E+00	-1.242 875 58E+00
b4	-1.061 146 392 6E+00	-4.975 131 465 9E-01	-4.587 885 26E-01	-4.654 521 71E-01	-4.851 613 02E-01	-5.079 250 93E-01	-5.309 124 33E-01
b5	3.827 859 278 7E+00	2.543 651 584 5E+00	2.458 352 30E+00	2.453 527 79E+00	2.473 069 37E+00	2.498 109 78E+00	2.523 821 38E+00
b6	-7.756 293 635 0E-01	-3.514 346 900 2E-01	-1.813 502 55E-01	-1.498 871 63E-01	-1.438 490 22E-01	-1.472 555 92E-01	-1.545 721 20E-01
b7	1.045 517 070 6E+01	4.621 358 937 5E+00	3.513 016 07E+00	3.347 812 09E+00	3.418 470 95E+00	3.570 412 09E+00	3.750 261 44E+00
b8	1.320 082 877 1E+00	1.248 327 500 3E+00	1.081 576 71E+00	1.120 461 83E+00	1.177 360 62E+00	1.236 087 00E+00	1.292 288 06E+00
b9	-2.960 658 687 9E+01	-1.530 065 544 8E+01	-1.289 312 11E+01	-1.229 595 15E+01	-1.225 191 17E+01	-1.241 651 73E+01	-1.266 591 48E+01
b10	-7.235 679 546 4E-01	-1.490 112 967 0E+00	-1.502 417 12E+00	-1.789 770 19E+00	-2.056 088 47E+00	-2.294 870 87E+00	-2.508 250 94E+00

(continue)

$q \in [0.7, 0.9]$							
(l, m)	(2,2)	(3,3)	(4,4)	(5,5)	(6,6)	(7,7)	(8,8)
a1	-1.023 713 029 8E+00	-1.166 658 087 1E+00	-1.222 731 64E+00	-1.248 720 50E+00	-1.261 912 67E+00	-1.268 916 07E+00	-1.272 669 58E+00
a2	-1.794 624 263 6E+00	-1.621 193 222 4E+00	-1.532 744 82E+00	-1.494 294 70E+00	-1.467 808 06E+00	-1.450 362 30E+00	-1.437 271 19E+00
a3	2.046 890 798 3E+01	1.390 712 770 5E+01	1.156 757 55E+01	1.019 439 43E+01	8.528 950 06E+00	7.003 335 05E+00	5.477 075 74E+00
a4	1.622 959 908 3E+01	5.362 947 562 0E+00	5.947 955 12E+00	5.707 37 817E+00	6.303 486 32E+00	6.799 447 78E+00	7.313 881 99E+00
a5	-5.004 421 387 0E+02	-3.347 118 008 8E+02	-4.131 285 79E+02	-4.485 704 81E+02	-5.149 144 18E+02	-5.758 377 07E+02	-6.368 303 10E+02
a6	6.231 165 980 4E+02	2.727 905 322 4E+02	2.709 958 22E+02	2.556 013 33E+02	2.651 145 53E+02	2.743 705 80E+02	2.850 99 738E+02
a7	-4.325 486 276 4E+03	-2.273 153 589 7E+03	-2.543 524 21E+03	-2.597 673 54E+03	-2.862 367 87E+03	-3.114 178 16E+03	-3.374 011 24E+03
a8	2.468 012 372 9E+03	1.040 409 109 8E+03	1.028 817 92E+03	9.628 231 50E+02	9.935 000 91E+02	1.026 086 92E+03	1.064 995 04E+03
a9	-3.485 493 596 2E+03	-1.544 287 152 3E+03	-1.661 606 93E+03	-1.639 724 14E+03	-1.772 818 93E+03	-1.904 164 59E+03	-2.043 409 99E+03
a10	1.125 528 084 9E+03	4.333 129 781 3E+02	4.330 127 02E+02	4.041 597 05E+02	4.188 420 50E+02	4.346 140 63E+02	4.530 582 73E+02
b1	-6.797 912 744 8E-01	-6.720 621 720 2E-01	-6.719 472 93E-01	-6.718 493 38E-01	-6.720 348 23E-01	-6.722 772 45E-01	-6.725 406 46E-01
b2	6.245 384 453 4E-01	5.521 354 590 0E-01	5.415 411 75E-01	5.362 353 71E-01	5.342 383 99E-01	5.335 163 53E-01	5.334 432 63E-01
b3	-2.475 298 992 1E+00	-1.873 194 636 0E+00	-1.705 390 52E+00	-1.666 136 31E+00	-1.668 274 80E+00	-1.686 228 89E+00	-1.709 546 37E+00
b4	1.063 403 909 0E+00	1.979 531 940 0E+00	2.015 068 06E+00	2.182 686 43E+00	2.350 0031 1E+00	2.510 300 61E+00	2.656 873 45E+00
b5	7.422 850 698 9E+00	1.859 844 594 6E+00	7.160 799 72E-01	-7.787 803 67E-02	-6.488 202 78E-01	-1.101 148 77E+00	-1.473 894 84E+00
b6	-2.387 763 519 0E+00	-5.235 497 761 7E+00	-5.733 668 92E+00	-6.398 077 14E+00	-7.011 680 91E+00	-7.569 716 51E+00	-8.068 740 97E+00
b7	-6.881 562 105 8E-01	6.911 189 730 0E+00	9.083 320 17E+00	1.103 847 16E+01	1.267 712 57E+01	1.408 284 62E+01	1.530 320 42E+01
b8	-9.954 888 325 3E-01	3.358 493 951 2E+00	4.225 884 47E+00	4.978 654 80E+00	5.602 755 55E+00	6.139 186 60E+00	6.604 012 24E+00
b9	-3.036 495 432 0E+01	-1.795 232 730 9E+01	-1.588 692 34E+01	-1.547 953 21E+01	-1.560 625 99E+01	-1.591 883 46E+01	-1.629 882 79E+01
b10	1.372 472 520 0E+01	2.847 195 462 5E-01	-2.918 044 29E+00	-5.002 550 10E+00	-6.517 913 10E+00	-7.717 042 63E+00	-8.705 299 80E+00

Tab. 5 Fitting results of $a_8^{\text{Hor,NS}}$, $a_{10}^{\text{Hor,NS}}$, $a_{12}^{\text{Hor,NS}}$ and coefficients for $a_{11}^{\text{Hor,S}}$, $a_{12}^{\text{Hor,S}}$

$a_8^{\text{Hor,NS}}$	5.237 253 010 7E+00	p_2	-2.696 214 919 4E+02	p_6	3.551 554 985 7E+02	p_{10}	1.291 757 498 0E+03
$a_{10}^{\text{Hor,NS}}$	-7.773 892 177 1E+01	p_3	8.997 620 335 5E+01	p_7	-1.590 451 617 6E+03	p_{11}	-2.091 788 653 0E+02
$a_{12}^{\text{Hor,NS}}$	4.511 589 427 8E+02	p_4	-3.841 746 785 7E+02	p_8	1.576 498 655 3E+03	p_{12}	-1.084 215 885 9E+03
p_1	3.770 790 555 0E+02	p_5	-7.961 912 247 1E+01	p_9	-9.284 185 336 1E+02	p_{13}	4.291 650 420 9E+02

References:

- [1] ALEXANDER T. Stellar processes near the massive black hole in the Galactic center[J]. *Phys. Rep.*, 2005, 419(2-3): 65-142.
- [2] OLTEAN M, SPUERTA C F, SPALLICCI A D A M. A frequency-domain implementation of the particle-without-particle approach to EMRIs[J]. *J. Phys. : Conf. Ser.*, 2017, 840:012056.
- [3] KHAN F M, BERCZIK P, JUST A. Gravitational wave driven mergers and coalescence time of supermassive black holes [J]. *Astronomy & Astrophysics*, 2018, A71:615.
- [4] GUO Z K, CAI R G, ZHANG Y ZH, *et al.*. Taiji program: gravitational-wave sources[R]. *arXiv*:2018, 1807:09495.
- [5] LUO J, CHEN L SH, DUAN H Z, *et al.*. TianQin: a space-borne gravitational wave detector[J]. *Class. Quantum Grav.*, 2016, 33(3): 035010.
- [6] FINN L S, THORNE K S. Gravitational waves from a compact star in a circular, inspiral orbit, in the equatorial plane of a massive, spinning black hole, as observed by LISA[J]. *Phys. Rev.*, 2000, 62:124021.
- [7] CUTLER C, THORNE K S. Proceedings of general relativity and gravitation XVI[C]. BISHPO N T, Singapore, World Scientific, 2002.
- [8] AMARO-SEOANE P, GAIR J R, FREITAG M, *et al.*. Astrophysics, detection and science applications of intermediate- and extreme mass-ratio inspirals[J]. *Class. Quantum Grav.*, 2007, 24:R113-R169.
- [9] GAIR J R, BARACK L, CREIGHTON T, *et al.*. Event rate estimates for LISA extreme mass ratio capture sources[J].

Class. Quantum Grav.,2004,21(20):S1595-S1606.

- [10] HOPMAN C,ALEXANDER T. The effect of mass segregation on gravitational wave sources near massive black holes[J]. *Astrophys. J. Letters*,2006,645(2):L133-L136.
- [11] BARACK L,CARDOSO V,NISSANKE S,*et al.*. Black holes, gravitational waves and fundamental physics;a roadmap [R]. arXiv:2018,1806:05195.
- [12] REGGE T,WHEELER J A. Stability of a schwarzschild singularity[J]. *Phys. Rev.*,1957,108(4):1063-1069.
- [13] TEUKOLSKY S A. Perturbations of a rotating black hole. I. fundamental equations for gravitational, electromagnetic, and neutrino-field perturbations[J]. *Astrophys. J.*,1973,185:635-647.
- [14] TEUKOLSKY S A,PRESS W H. Perturbations of a rotating black hole. III-Interaction of the hole with gravitational and electromagnetic radiation[J]. *Astrophys. J.*,1974,193:443-461.
- [15] GAIR J R,GLAMPEDAKIS K. Improved approximate inspirals of test bodies into Kerr black holes[J]. *Phys. Rev.*,2006,73(6):064037.
- [16] BABAK S,FANG H,GAIR J R,*et al.*. “Kludge” gravitational waveforms for a test-body orbiting a Kerr black hole[J]. *Phys. Rev D*,2007,75(2):024005.
- [17] BIERI L,YUNES N,GARFINKLE D. Gravitational waves and their mathematics[J]. *AMS Notices*,2017,64(7):693-708.
- [18] GLAMPEDAKIS K,HUGHES S A,KENNEFICK D. Approximating the inspiral of test bodies into Kerr black holes[J]. *Phys. Rev. D*,2002,66(6):064005.
- [19] TARACCHINI A,BUONANNO A,PAN Y,*et al.*. Effective-one-body model for black-hole binaries with generic mass ratios and spins[J]. *Phys. Rev.*,2014,89(6):061502.
- [20] PÜRRER M. Frequency domain reduced order model of aligned-spin effective-one-body waveforms with generic mass ratios and spins[J]. *Phys. Rev.*,2016,93(6):064041.
- [21] ABBOTT B P,ABBOTT R,ABBOTT T D,*et al.*. Binary black hole mergers in the first advanced LIGO observing run [J]. *Phys. Rev X*,2016,6(4):041015.
- [22] YUNES N,BUONANNO A,HUGHES S A,*et al.*. Modeling extreme mass ratio inspirals within the effective-one-body approach[J]. *Phys. Rev. Lett.*,2010,104(9):091102.
- [23] YUNES N,BUONANNO A,HUGHES S A,*et al.*. Extreme mass-ratio inspirals in the effective-one-body approach:Quasicircular, equatorial orbits around a spinning black hole[J]. *Phys. Rev.*,2013,83(10):109904.
- [24] CUTLER C,FINN L S,POISSON E,*et al.*. Gravitational radiation from a particle in circular orbit around a black hole. II. numerical results for the nonrotating case[J]. *Phys. Rev.*,1993,47(3):1511-1518.
- [25] POISSON E. Gravitational radiation from a particle in circular orbit around a black hole. VI. accuracy of the post-Newtonian expansion[J]. *Phys. Rev.*,1995,52(10):5719-5723.
- [26] DAMOUR T,IYER B R,SATHYAPRAKASH B S. Improved filters for gravitational waves from inspiralling compact binaries[J]. *Phys. Rev.*,1998,57(2):885-907.
- [27] PAN Y,BUONANNO A,FUJITA R,*et al.*. Post-Newtonian factorized multipolar waveforms for spinning, nonprecessing black-hole binaries[J]. *Phys. Rev.*,2011,83(6):064003.
- [28] DAMOUR T,IYER B R,NAGAR A. Improved resummation of post-newtonian multipolar waveforms from circularized compact binaries[J]. *Phys. Rev.*,2009,79(6):064004.
- [29] DAMOUR T,NAGAR A. Faithful effective-one-body waveforms of small-mass-ratio coalescing black hole binaries[J]. *Phys. Rev.*,2007,76(6):064028.
- [30] TARACCHINI A,PAN Y,BUONANNO A,*et al.*. Prototype effective-one-body model for nonprecessing spinning inspiral-merger-ringdown waveforms[J]. *Phys. Rev.*,2012,86(2):024011.
- [31] BABAK S,TARACCHINI A,BUONANNO A. Validating the effective-one-body model of spinning, precessing binary black holes against numerical relativity[J]. *Phys. Rev.*,2017,95(2):024010.
- [32] JARANOWSKI P,KRLAK A. Gravitational-wave data analysis. formalism and sample applications;the gaussian case

- [J]. *Living Reviews in Relativity*, 2005, 8:3.
- [33] MINO Y, SASAKI M, SHIBATA M, *et al.*. Chapter 1. *Black Hole Perturbation*[M]. *Prog. Theor. Phys.*, 1997, 128:1-121.
- [34] HAN W B. Fast evolution and waveform generator for extreme-mass-ratio inspirals in equatorial-circular orbits[J]. *Class. Quantum Grav.*, 2016, 33(6):065009.
- [35] HAN W B. Gravitational radiation from a spinning compact object around a supermassive Kerr black hole in circular orbit[J]. *Phys. Rev.*, 2010, 82(8):084013.
- [36] HAN W B, CAO Z J. Constructing effective one-body dynamics with numerical energy flux for intermediate-mass-ratio inspirals[J]. *Phys. Rev.*, 2011, 84(4):044014.
- [37] HAN W B. Gravitational waves from extreme-mass-ratio inspirals in equatorially eccentric orbits[J]. *International Journal of Modern Physics D*, 2014, 23(7):1450064.

作者简介:



程 然(1988—),男,内蒙呼伦贝尔人,博士研究生,主要从事低频引力波源数值模拟方面的研究。E-mail:chengran@shao.ac.cn



韩文标(1980—),男,安徽巢湖人,博士,研究员,主要从事低频引力波源的数值模拟、分析建模,利用引力波信号反演源的天体物理性质,检验引力理论和研究宇宙学等方面的研究。E-mail:wbhan@shao.ac.cn